Coordinated Control of DFIG Converters to Comply with Reactive Current Requirements in Emerging Grid Codes

Yuanzhu Chang, *Member*, *IEEE*, Ilhan Kocar, *Senior Member*, *IEEE*, Jiabing Hu, *Senior Member*, *IEEE*, Ulas Karaagac, *Member*, *IEEE*, Ka Wing Chan, *Member*, *IEEE*, and Jean Mahseredjian, *Fellow*, *IEEE*

***Abstract*—The doubly-fed induction generator (DFIG) is considered to provide a low-reactance path in the negative-sequence system and naturally comply with requirements on the negative-sequence reactive current in emerging grid codes. This paper shows otherwise and how the control strategy of converters plays a key role in the formation of the active and reactive current components. After investigating the existing control strategies from the perspective of grid code compliance and showing how they fail in addressing emerging requirements on the negative-sequence reactive current, we propose a new coordinated control strategy that complies with reactive current requirements in grid codes in the positive- and negative-sequence systems. The proposed method fully takes advantage of the current and voltage capacities of both the rotor-side converter (RSC) and grid-side converter (GSC), which enables the grid code compliance of the DFIG under unbalanced three-phase voltages due to asymmetrical faults. The mathematical investigations and proposed strategy are validated with detailed simulation models using the Electric Power Research Institute (EPRI) benchmark system. The derived mathematical expressions provide analytical clarifications on the response of the DFIG in the negative-sequence system from the grid perspective.**

***Index Terms*—Doubly-fed induction generator (DFIG), negative sequence, short circuit, wind turbine generator, reactive current, space vector, unbalanced fault, phase lock loop (PLL).**

NOMENCLATURE

A. Variables

θ_a, θ_b, θ_c	Phase angles of three-phase quantities
θ_{U+}	Initial phase of positive-sequence voltage
θ_{V-}	Angle of negative-sequence voltage vector in negative phase lock loop (PLL) reference frame
σ	Leakage factor
$\boldsymbol{\psi}_s$, $\boldsymbol{\psi}_r$	Stator and rotor flux linkage vectors
ω_1	Synchronous angular velocity
ω_r, θ_r	Angular velocity and angle of rotor
ω_{PLL}, θ_{PLL}	Angular velocity and angle of PLL
$\boldsymbol{I}_s$, $\boldsymbol{I}_r$	Current vectors of stator and rotor
$\boldsymbol{I}_g$, $\boldsymbol{I}_{WTG}$	Current vectors of grid-side converter (GSC) and wind turbine generator (WTG)
$I_{\mathrm{RSC,max}}$	The maximum current of rotor-side converter (RSC)
$I_{\mathrm{GSC,max}}$	The maximum current of GSC
I1A, I1R	Positive-sequence active and reactive currents
I2A, I2R	Negative-sequence active and reactive currents
K_{V+}, K_{V-}	Coefficients for I1R and I2R injections
$K_{pi,\mathrm{RSC}}$, $K_{ii,\mathrm{RSC}}$	Proportional and integral parameters of RSC current control
$K_{pi,\mathrm{GSC}}$, $K_{ii,\mathrm{GSC}}$	Proportional and integral parameters of GSC current control
$K_{p,\mathrm{PLL}}$, $K_{i,\mathrm{PLL}}$	Proportional and integral parameters of PLL control
L_s, L_r, L_m	Stator, rotor, and magnetizing inductances
L_{choke}	Inductance of choke filter of GSC
N_r/N_s	Turn ratio between rotor and stator windings
P, Q	Active and reactive power
R_s, R_r	Stator and rotor resistances
s	Slip
$\boldsymbol{U}_s$, $\boldsymbol{U}_r$	Voltage vectors of stator and rotor
U_B, S_B	Voltage and power references of per-unit values

B. Superscripts

$*$	Reference value
$\overline{(\cdot)}$	Conjugate complex

Manuscript received: March 19, 2021; revised: June 26, 2021; accepted: September 28, 2021. Date of CrossCheck: September 28, 2021. Date of online publication: December 22, 2021.

Y. Chang, I. Kocar (corresponding author), and J. Mahseredjian are with the Electrical Engineering Department, Polytechnique Montréal, Montréal, Canada (e-mail: yuanzhu.chang@polymtl.ca; ilhan.kocar@polymtl.ca; jean.mahseredjian@polymtl.ca).

J. Hu is with the School of Electrical and Electronic Engineering, Huazhong University of Science and Technology, Wuhan 430074, China (e-mail: j.hu@hust.edu.cn).

U. Karaagac and K. W. Chan are with the Department of Electrical Engineering, The Hong Kong Polytechnic University, Hong Kong, China (e-mail: kevin.kw.chan@polyu.edu.hk; ulas.karaagac@polyu.edu.hk).

DOI: 10.35833/MPCE.2021.000191

abc, *αβ*	Three- and two-phase reference frames
dq+, *dq* –	Positive and negative synchronous reference frames rotating at ω_1 and $-\omega_1$
PLL +, *PLL* –	Positive and negative PLL reference frames
SVR –	Negative-sequence stator voltage reference

C. Subscripts

+, –	Positive- and negative-sequence components
d, *q*	*d*- and *q*-axis projections of vector
g, *WTG*	GSC and WTG
in, out	Before and after limiter
s, *r*	Stator and rotor

I. Introduction

WIND turbine generators (WTGs) play a key role in the decarbonization of power grids and there is a worldwide increase in the share of these renewable energy sources in the generation fleet of power grids. Wind parks (WPs) consisting of WTGs should comply with a series of grid interconnection requirements introduced by grid codes [1]-[3].

Early grid codes [4]-[6] require WPs to remain connected to the power grid within defined limits specified by voltage-versus-time curves and to continue operating as specified during a voltage disturbance. The goal is for WPs to contribute to the conservation of active power balance after fault clearance. In addition, several grid codes introduce the requirements on the contribution of additional positive-sequence reactive current (I1R) from WPs [7], [8]. In this way, WPs could support the system positive-sequence voltage and thus contribute to power system transient stability [9], [10]. Recent grid codes, such as the ones of Germany and China [11] - [13], introduce the requirements on the negative-sequence reactive current (I2R) from WPs. Under this requirement, a WP mimics a shunt reactor in the negative-sequence system, as shown in Fig. 1 [12], and this would be desirable for grid operation since it will limit voltage unbalance under asymmetrical faults [14]. This is also favorable to protect equipment sensitive to negative-sequence voltages or ensure the operation of protective devices relying on negative-sequence currents [15]-[18].

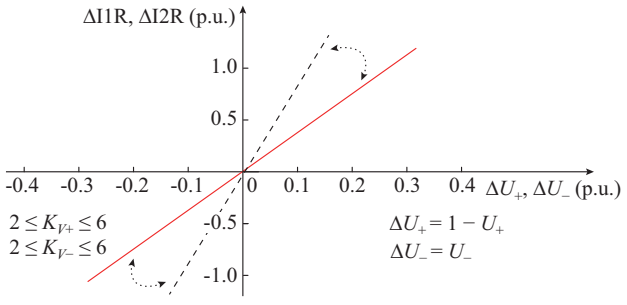

Fig. 1. Additional (Δ) I1R and I2R requirements in German grid code versus variation in voltage in positive- and negative-sequence systems.

There is a number of studies on the control of doubly-fed induction generator (DFIG)-based WTGs (also referred to as Type-III WTGs) to meet fault ride through (FRT) requirements including grid connection and I1R injection requirements [19]-[22]. The control of the DFIG under unbalanced conditions and the coordination of converters to reduce the mechanical stress have been studied in [23], [24]. However, studies focusing on the controlled I2R injection to the grid are mainly related to the full-size converter (FSC) based WTGs (also referred to as Type-IV WTGs) [25]-[27] except the study presented in [28] focusing on DFIG-based WTGs.

In [25], a generic electromagnetic transient-type (EMT-type) model of an FSC-based WTG is presented considering a decoupled sequence control scheme for the control of the I2R component. Reference [26] discusses the calculation of current references and limiters for generators coupled to the grid through voltage source converters (VSCs), such as the FSC, to comply with I1R and I2R requirements. The injection of reactive power in the positive- and negative-sequence systems is favorable for the grid as opposed to an injection in positive sequence only [27].

Given that the stator winding of the DFIG is directly coupled to the grid, a DFIG-based WTG is simply regarded as a squirrel-cage induction machine (IM) or replaced with a fixed impedance (mainly reactive) as in [29], regardless of the impact of converters' control. From this point of view, the DFIG provides a low reactance path in the negative-sequence system that would naturally comply with I2R requirements. However, this assumption is not even accurate during crowbar protection because of the slip and resistance of the crowbar [30].

The impact of control strategies on the fault current of the DFIG has been shown to be important and plays a role in circuit breaker ratings and protection settings [31]-[33]. However, to the best of authors' knowledge, its I2R characteristics have not been discussed in detail from the grid perspective considering different control strategies and emerging grid codes.

The existing I2R control strategies proposed for the FSC-based WTGs cannot be transferred to the DFIG-based WTGs owing to their differences in topology. The complexity and challenges are as follows.

1) Extra degree of freedom: the FSC is interfaced to the grid through its grid-side converter (GSC), which in consequence supplies all the fault current from WTG. The fault current of DFIG-based WTG consists of the GSC current as well as the stator current that is governed by its rotor-side converter (RSC). To generate I1R and I2R components in compliance with grid codes, eight different current references need to be coordinated, namely the active and reactive currents of the RSC and GSC in the positive- and negative-sequence systems.

2) Reduced (non-full) size converters: the GSC of the FSC is designed to convert the rated voltage and current, whereas the RSC and GSC of the DFIG are both rated to convert the slip power (typically 30% of the rated power) [34]. Thus, the control implementation should fully consider the limitations in current and voltage regulation capacity of the converters. According to [35], given the reduced capacity of its converters, the DFIG can hardly generate the required I1R with the existing negative-sequence control schemes when the negative-sequence voltage is greater than 0.1 p.u..

3) Special control configurations: apart from the classical balanced positive-sequence control (BPSC), a well-known control strategy for DFIG-based WTGs under unbalanced voltages is to generate negative-sequence currents through the RSC to eliminate the double grid frequency oscillations in electromagnetic torque (Tem) [23]. This control strategy is referred to as the positive- and negative-sequence control focusing on Tem and denoted by PNSC-Tem in this paper. Reference [28] proposes a coordinated control of DFIG converters on the basis of PNSC-Tem, in which the GSC is used to provide I2R to the grid under small voltage unbalances. This coordinated control strategy is denoted as the existing coordinated control in this paper. Note that, the current injection of a DFIG-based WTG operated under the existing control strategies has not been studied yet from the perspective of grid code compliance in the negative-sequence system.

This paper has two main contributions. We first derive detailed mathematical expressions of WTG currents in the positive- and negative-sequence systems under existing control strategies. The objective is to fill the gap of knowledge regarding the DFIG's detailed behaviors in the negative-sequence system from the grid perspective. Then, we propose a new coordinated control scheme for DFIG converters, called flexible control of the reactive current in the positive- and negative-sequence systems and denoted by PNSC-I12R, to comply with I1R and I2R requirements in emerging grid codes under practical unbalanced voltages following asymmetrical faults on the grid.

The remainder of this paper is organized as follows. Section II briefly introduces the space vector notation and then deduces mathematical equations governing the behavior of IM of DFIG in the positive- and negative-sequence systems. In Section III, the existing control strategies for DFIG-based WTGs are introduced. In Sections IV and V, the positive- and negative-sequence currents of the DFIG are analyzed under the existing strategies. The new coordinated control scheme PNSC-I12R is proposed in Section VI. In Section VII, the performances of DFIG-based WTGs under the existing and proposed control strategies are compared by simulations. Finally, conclusions are drawn in Section VIII.

II. DFIG in Positive- and Negative-sequence Systems

This section briefly presents the space vector notation used in this paper and then develops basic equations of the IM in the positive- and negative-sequence systems. Further details on space vector theory and dynamic modeling of DFIG are available in [36] and [37].

A. Vector Expressions of Asymmetrical Quantities

In the steady state, the frequency of the three-phase voltages, currents, and flux linkages are the same as the grid frequency. A generic set of three-phase variables is considered, which is expressed as:

$$\begin{cases} x_a = X_a \cos(\omega_1 t + \theta_a) \\ x_b = X_b \cos(\omega_1 t + \theta_b) \\ x_c = X_c \cos(\omega_1 t + \theta_c) \end{cases} \tag{1}$$

where x stands for the instantaneous value; and X stands for the magnitude.

Due to the three-phase transformer connection in WPs, there is no zero-sequence component in the voltages, currents, or flux linkages of the DFIG. By applying the Clark transformation, the variables can be transformed into the two-phase stationary reference ($\alpha\beta$) as:

$$\begin{bmatrix} x_\alpha \\ x_\beta \end{bmatrix} = \frac{2}{3} \begin{bmatrix} 1 & -\frac{1}{2} & -\frac{1}{2} \\ 0 & \frac{\sqrt{3}}{2} & -\frac{\sqrt{3}}{2} \end{bmatrix} \begin{bmatrix} x_a \\ x_b \\ x_c \end{bmatrix} \tag{2}$$

By rewriting (2) in the space vector form and then applying symmetrical components [38], the vector measured in the $\alpha\beta$ frame is:

$$\boldsymbol{X}^{\alpha\beta} = x_\alpha + \mathrm{j}x_\beta = \boldsymbol{X}_+^{\alpha\beta} + \boldsymbol{X}_-^{\alpha\beta} \tag{3}$$

$$\begin{cases} \boldsymbol{X}_+^{\alpha\beta} = \boldsymbol{X}_+^{dq+} \mathrm{e}^{\mathrm{j}\omega_1 t} \\ \boldsymbol{X}_+^{dq+} = X_{d+} + \mathrm{j}X_{q+} = X_+ \mathrm{e}^{\mathrm{j}\theta_+} \end{cases} \tag{4}$$

$$\begin{cases} \boldsymbol{X}_-^{\alpha\beta} = \boldsymbol{X}_-^{dq-} \mathrm{e}^{-\mathrm{j}\omega_1 t} \\ \boldsymbol{X}_-^{dq-} = X_{d-} + \mathrm{j}X_{q-} = X_- \mathrm{e}^{-\mathrm{j}\theta_-} \end{cases} \tag{5}$$

$$\begin{bmatrix} X_+ \mathrm{e}^{\mathrm{j}\theta_+} \\ X_- \mathrm{e}^{\mathrm{j}\theta_-} \end{bmatrix} = \frac{1}{3} \begin{bmatrix} 1 & \mathrm{e}^{\mathrm{j}\frac{2\pi}{3}} & \mathrm{e}^{-\mathrm{j}\frac{2\pi}{3}} \\ 1 & \mathrm{e}^{-\mathrm{j}\frac{2\pi}{3}} & \mathrm{e}^{\mathrm{j}\frac{2\pi}{3}} \end{bmatrix} \begin{bmatrix} X_a \mathrm{e}^{\mathrm{j}\theta_a} \\ X_b \mathrm{e}^{\mathrm{j}\theta_b} \\ X_c \mathrm{e}^{\mathrm{j}\theta_c} \end{bmatrix} \tag{6}$$

In this paper, vectors are represented in italic and bold type. The superscript indicates the reference frame that the vector is measured.

The above expressions indicate that three-phase voltages, currents, and flux linkages of a DFIG can be regarded as the superposition of projections of a positive-sequence vector rotating at ω_1 and a negative-sequence vector rotating at $-\omega_1$. The locus of the resultant vector is an ellipse [36], as shown in Fig. 2.

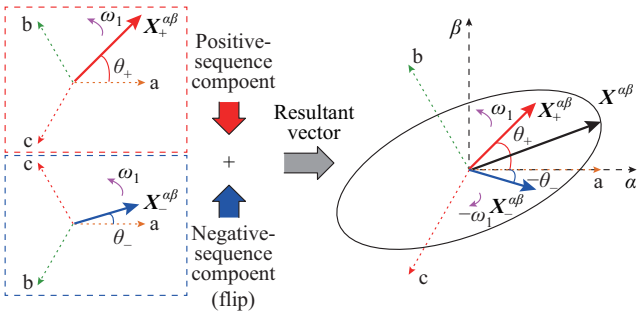

Fig. 2. Asymmetrical three-phase variables and their space vector expressions.

By changing the reference frame from $\alpha\beta$ to $dq+$ and $dq-$, the vector measurements become:

$$\boldsymbol{X}^{dq+} = \boldsymbol{X}^{\alpha\beta} \mathrm{e}^{-\mathrm{j}\omega_1 t} = \boldsymbol{X}_+^{dq+} + \boldsymbol{X}_-^{dq-} \mathrm{e}^{-\mathrm{j}2\omega_1 t} \tag{7}$$

$$\boldsymbol{X}^{dq-} = \boldsymbol{X}^{\alpha\beta} \mathrm{e}^{\mathrm{j}\omega_1 t} = \boldsymbol{X}_-^{dq-} + \boldsymbol{X}_+^{dq+} \mathrm{e}^{\mathrm{j}2\omega_1 t} \tag{8}$$

The equations indicate that, in the $dq+$ frame, positive-sequence components correspond to a stationary vector, and

the negative-sequence components correspond to a vector rotating with $-2\omega_1$.

B. Basic Equations of DFIG

In the $\alpha\beta$ frame, using the motor convention, the dynamic model of the DFIG can be expressed in the space vector form as:

$$\begin{cases} \boldsymbol{U}_s^{\alpha\beta} = R_s \boldsymbol{I}_s^{\alpha\beta} + \mathrm{d}\boldsymbol{\psi}_s^{\alpha\beta}/\mathrm{d}t \\ \boldsymbol{U}_r^{\alpha\beta} = R_r \boldsymbol{I}_r^{\alpha\beta} - \mathrm{j}\omega_r \boldsymbol{\psi}_r^{\alpha\beta} + \mathrm{d}\boldsymbol{\psi}_r^{\alpha\beta}/\mathrm{d}t \end{cases} \tag{9}$$

By substituting (3) into (9), the dynamics can be decomposed into positive- and negative-sequence quantities as:

$$\begin{cases} \boldsymbol{U}_{s+}^{\alpha\beta} = R_s \boldsymbol{I}_{s+}^{\alpha\beta} + \mathrm{d}\boldsymbol{\psi}_{s+}^{\alpha\beta}/\mathrm{d}t \\ \boldsymbol{U}_{r+}^{\alpha\beta} = R_r \boldsymbol{I}_{r+}^{\alpha\beta} - \mathrm{j}\omega_r \boldsymbol{\psi}_{r+}^{\alpha\beta} + \mathrm{d}\boldsymbol{\psi}_{r+}^{\alpha\beta}/\mathrm{d}t \end{cases} \tag{10}$$

$$\begin{cases} \boldsymbol{U}_{s-}^{\alpha\beta} = R_s \boldsymbol{I}_{s-}^{\alpha\beta} + \mathrm{d}\boldsymbol{\psi}_{s-}^{\alpha\beta}/\mathrm{d}t \\ \boldsymbol{U}_{r-}^{\alpha\beta} = R_r \boldsymbol{I}_{r-}^{\alpha\beta} - \mathrm{j}\omega_r \boldsymbol{\psi}_{r-}^{\alpha\beta} + \mathrm{d}\boldsymbol{\psi}_{r-}^{\alpha\beta}/\mathrm{d}t \end{cases} \tag{11}$$

C. Positive-sequence Equations of DFIG

By substituting (4) into (10), the model in the positive-sequence system is obtained as:

$$\begin{cases} \boldsymbol{U}_{s+}^{dq+} = R_s \boldsymbol{I}_{s+}^{dq+} + \mathrm{j}\omega_1 \boldsymbol{\psi}_{s+}^{dq+} + \mathrm{d}\boldsymbol{\psi}_{s+}^{dq+}/\mathrm{d}t \\ \boldsymbol{U}_{r+}^{dq+} = R_r \boldsymbol{I}_{r+}^{dq+} + \mathrm{j}s\omega_1 \boldsymbol{\psi}_{r+}^{dq+} + \mathrm{d}\boldsymbol{\psi}_{r+}^{dq+}/\mathrm{d}t \end{cases} \tag{12}$$

$$s = (\omega_1 - \omega_r)/\omega_1 \tag{13}$$

Since positive-sequence components correspond to a stationary vector in the $dq+$ frame, it is possible to remove the derivation terms in (12). By further ignoring the voltage drop on resistances, the positive-sequence quantities become:

$$\begin{cases} \boldsymbol{U}_{s+}^{dq+} \approx \mathrm{j}\omega_1 \boldsymbol{\psi}_{s+}^{dq+} = \mathrm{j}\omega_1 (L_s \boldsymbol{I}_{s+}^{dq+} + L_m \boldsymbol{I}_{r+}^{dq+}) \\ \boldsymbol{U}_{r+}^{dq+}/s \approx \mathrm{j}\omega_1 \boldsymbol{\psi}_{r+}^{dq+} = \mathrm{j}\omega_1 (L_m \boldsymbol{I}_{s+}^{dq+} + L_r \boldsymbol{I}_{r+}^{dq+}) \end{cases} \tag{14}$$

D. Negative-sequence Equations of DFIG

By substituting (5) into (11), the model in the negative-sequence system is obtained as:

$$\begin{cases} \boldsymbol{U}_{s-}^{dq-} = R_s \boldsymbol{I}_{s-}^{dq-} - \mathrm{j}\omega_1 \boldsymbol{\psi}_{s-}^{dq-} + \mathrm{d}\boldsymbol{\psi}_{s-}^{dq-}/\mathrm{d}t \\ \boldsymbol{U}_{r-}^{dq-} = R_r \boldsymbol{I}_{r-}^{dq-} - \mathrm{j}(2-s)\omega_1 \boldsymbol{\psi}_{r-}^{dq-} + \mathrm{d}\boldsymbol{\psi}_{r-}^{dq-}/\mathrm{d}t \end{cases} \tag{15}$$

If the derivation terms are removed and the voltage drop on resistances are neglected, the negative-sequence quantities become:

$$\begin{cases} \boldsymbol{U}_{s-}^{dq-} \approx -\mathrm{j}\omega_1 \boldsymbol{\psi}_{s-}^{dq-} = -\mathrm{j}\omega_1 (L_s \boldsymbol{I}_{s-}^{dq-} + L_m \boldsymbol{I}_{r-}^{dq-}) \\ \boldsymbol{U}_{r-}^{dq-}/(2-s) \approx -\mathrm{j}\omega_1 \boldsymbol{\psi}_{r-}^{dq-} = -\mathrm{j}\omega_1 (L_m \boldsymbol{I}_{s-}^{dq-} + L_r \boldsymbol{I}_{r-}^{dq-}) \end{cases} \tag{16}$$

III. The Existing Control Strategies of DFIG-based WTGs

This section briefly introduces the existing control strategies in terms of space vector orientations, current reference generations, priority level settings, and inner-loop controllers.

A. BPSC

The control strategies of the RSC and GSC are designed to independently regulate the active power and reactive power [39]. The BPSC, also classified as a vector control strategy in [40], is designed to regulate positive-sequence quantities. It is built either on the stator voltage orientation (SVO) or the stator flux orientation (SFO). Since there is no difference in terms of the steady-state performance [40], this paper studies the BPSC under SVO.

To achieve SVO, the BPSC employs a synchronous reference frame phase lock loop (SRF-PLL) to keep the d-axis of the control reference frame (denoted as $PLL+$) oriented along the positive-sequence voltage vector. A basic block diagram of the SRF-PLL is shown in Fig. 3.

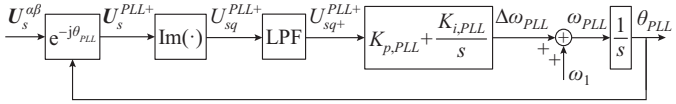

Fig. 3. Basic block diagram of SRF-PLL.

When SVO is achieved, the angles of the $PLL+$ with respect to the $\alpha\beta$ and $dq+$ frames are:

$$\begin{cases} \theta_{PLL} = \theta_{U+} + \omega_1 t \\ \Delta\theta_{PLL} = \theta_{PLL} - \omega_1 t = \theta_{U+} \end{cases} \tag{17}$$

Moreover, according to (5) and (17), the measurements of the positive- and negative-sequence vectors in the $PLL+$ are:

$$\boldsymbol{X}_+^{PLL+} = \boldsymbol{X}_+^{\alpha\beta} \mathrm{e}^{-\mathrm{j}\theta_{PLL}} = \boldsymbol{X}_+^{dq+} \mathrm{e}^{-\mathrm{j}\theta_{U+}} \tag{18}$$

$$\boldsymbol{X}_-^{PLL+} = \boldsymbol{X}_-^{\alpha\beta} \mathrm{e}^{-\mathrm{j}\theta_{PLL}} = \boldsymbol{X}_-^{dq-} \mathrm{e}^{-\mathrm{j}2\omega_1 t} \mathrm{e}^{-\mathrm{j}\theta_{U+}} \tag{19}$$

According to (19), the negative-sequence voltage vector introduces a 120 Hz oscillation to U_{sq}^{PLL+}. A low-pass filter (LPF) is adopted to filter this disturbance.

Under SVO, the positive-sequence voltage vector is:

$$\begin{cases} U_{sd+}^{PLL+} = U_+ \\ U_{sq+}^{PLL+} = 0 \end{cases} \tag{20}$$

The positive-sequence active and reactive power at the stator and GSC sides are:

$$P_{s+} + \mathrm{j}Q_{s+} = \boldsymbol{U}_{s+}^{PLL+} \bar{\boldsymbol{I}}_{s+}^{PLL+} = U_+ I_{sd+}^{PLL+} - \mathrm{j}U_+ I_{sq+}^{PLL+} \tag{21}$$

$$P_{g+} + \mathrm{j}Q_{g+} = \boldsymbol{U}_{s+}^{PLL+} \bar{\boldsymbol{I}}_{g+}^{PLL+} = U_+ I_{gd+}^{PLL+} - \mathrm{j}U_+ I_{gq+}^{PLL+} \tag{22}$$

where I_{gd+}^{PLL+} and I_{sd+}^{PLL+} are the positive-sequence active currents at the GSC and stator sides, respectively; and I_{gq+}^{PLL+} and I_{sq+}^{PLL+} are the positive-sequence reactive currents at the GSC and stator sides, respectively.

If FRT is activated, the required I1R in grid codes I_{WTGq+}^{PLL+} is typically given by:

$$I_{WTGq+}^{PLL+} = I_{sq+}^{PLL+} + I_{gq+}^{PLL+} = K_{V+}(1 - U_+) \tag{23}$$

The I1R is first contributed from the stator side (controlled by the RSC). By substituting (23) into (14), the required positive-sequence rotor current reference (before the limiter) $I_{rq,\mathrm{in}+}^{PLL+*}$ is:

$$I_{rq,\mathrm{in}+}^{PLL+*} = -\frac{L_s}{L_m} I_{sq+}^{PLL+} - \frac{U_+}{\omega_1 L_m} = -\frac{L_s}{L_m} K_{V+}(1 - U_+) - \frac{U_+}{\omega_1 L_m} \tag{24}$$

If the current reference in (24) is greater than the RSC current capacity, the GSC will generate the remaining I1R $I_{gq,\mathrm{in}+}^{PLL+*}$ as:

$$I_{gq,\text{in}+}^{PLL+*}=K_{V+}(1-U_+)+\frac{U_+}{\omega_1 L_s}+\frac{L_m}{L_s}I_{rq,\text{out}+}^{PLL+*} \tag{25}$$

Different from the normal operation, the priority is switched to reactive current during FRT as shown in Fig. 4, where level-1 indicates the highest priority.

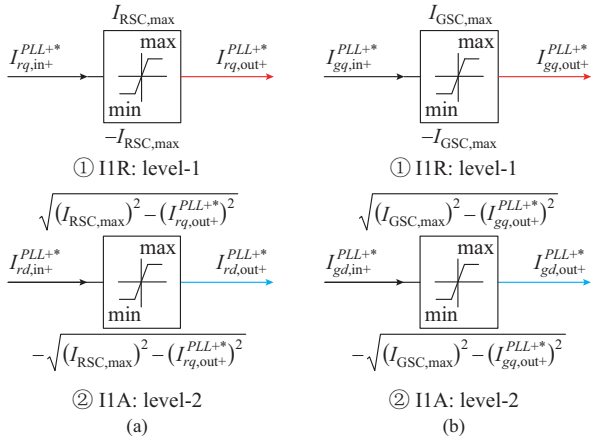

Fig. 4. Limiter and priority settings of BPSC during FRT. (a) RSC. (b) GSC.

To realize the four positive-sequence current references in Fig. 4, four coupled inner-loop controllers are employed in the RSC and GSC. After being organized in space vector form, their basic block diagrams are given in Fig. 5.

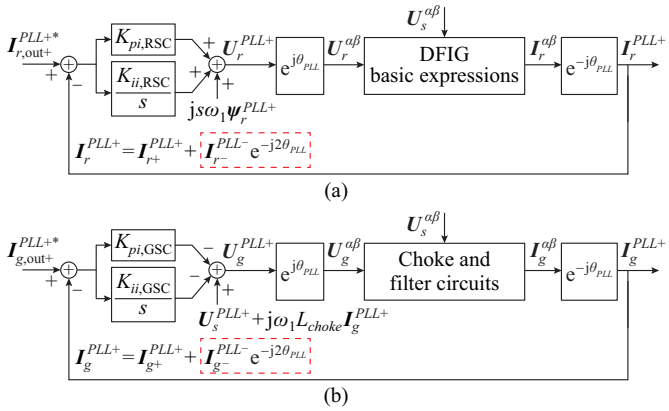

Fig. 5. Coupled inner-loop control in BPSC. (a) RSC. (b) GSC.

The impact of negative-sequence currents on the coupled inner-loop control should be highlighted here. As given in (19), negative-sequence currents introduce 120 Hz disturbances in measurements (marked by red dotted block in Fig. 5). As a result, negative-sequence voltages will be generated by these controllers. This impact will be analyzed in detail later in Section IV-B.

B. PNSC-Tem and the Existing Coordinated Control

The PNSC-Tem is designed to independently control the positive- and negative-sequence quantities. This paper also studies the PNSC-Tem under SVO as a general case.

To decompose the sequence quantities from measurements, a decoupled double synchronous reference frame phase lock loop (DDSRF-PLL) [39] or other estimation elements [41] can be used to provide a positive synchronous control reference frame ($PLL+$) and a negative synchronous control reference frame ($PLL-$). $PLL+$ orients along the positive-sequence voltage vector, while $PLL-$ is the reverse of $PLL+$. Figure 6 shows the basic block diagram of the DDSRF-PLL used in this paper.

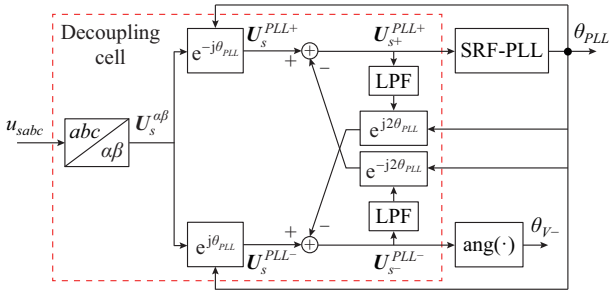

Fig. 6. Basic block diagram of DDSRF-PLL.

The positive-sequence current references of the PNSC-Tem strategy are the same as those of the BPSC. In addition, the negative-sequence rotor current references of the PNSC-Tem are carefully designed to eliminate the double grid frequency oscillations in Tem [23]. These rotor current references can be rewritten in space vector form as:

$$\boldsymbol{I}_{r-}^{PLL-*}=\boldsymbol{U}_{s-}^{PLL-}\bar{\boldsymbol{I}}_{r+}^{PLL+*}/U_+ \tag{26}$$

Based on (26), the magnitude relationship between positive- and negative-sequence rotor currents is expressed as:

$$\left|\boldsymbol{I}_{r-}^{PLL-*}\right|=\frac{U_-}{U_+}\left|\bar{\boldsymbol{I}}_{r+}^{PLL+*}\right|=\frac{U_-}{U_+}\left|\boldsymbol{I}_{r+}^{PLL+*}\right| \tag{27}$$

To avoid overcurrent, the current limitation and priority level are set as Fig. 7. According to (27), the allocation factor p_1 is:

$$p_1=U_+/(U_++U_-) \tag{28}$$

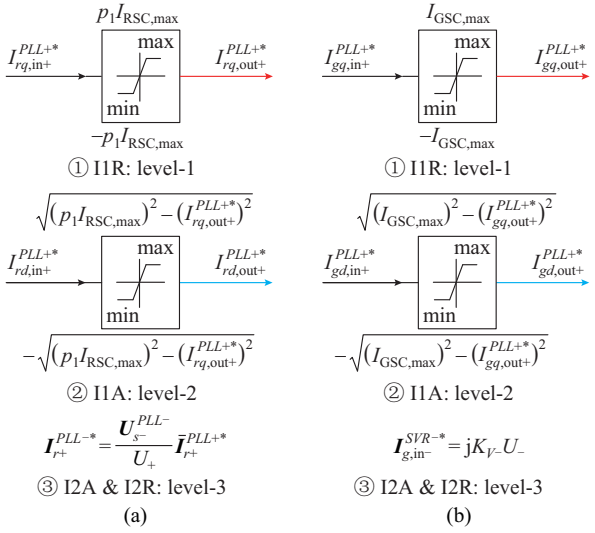

Fig. 7. Limiter and priority settings of PNSC-Tem and existing coordinated control during FRT. (a) RSC. (b) GSC.

In addition to the PNSC-Tem, the negative-sequence current references of GSC have been used in the existing coordinated control strategy to provide I2R. In [28], the negative-

sequence current references of GSC are given by:

$$\boldsymbol{I}_{\mathrm{g,in}-}^{SVR-*}=\mathrm{j}K_{V-}U_{-} \tag{29}$$

To realize these eight current references in Fig. 7, eight decoupled inner-loop controllers are employed as shown in Figs. 8 and 9. As opposed to the BPSC strategy, the positive- and negative-sequence quantities won't influence each other by introducing 120 Hz disturbances in measurements.

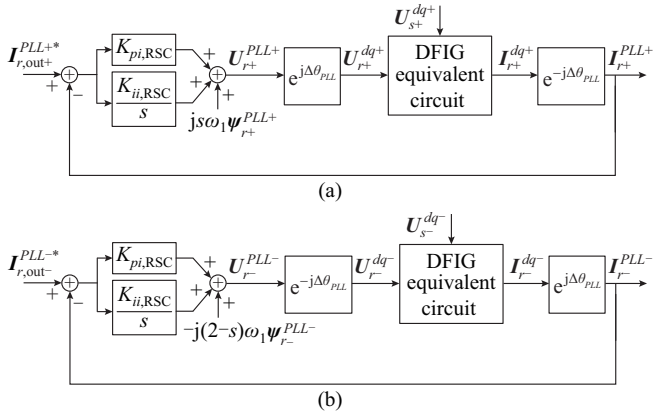

Fig. 8. Decoupled inner-loop control of RSC in PNSC-Tem. (a) Positive sequence. (b) Negative sequence.

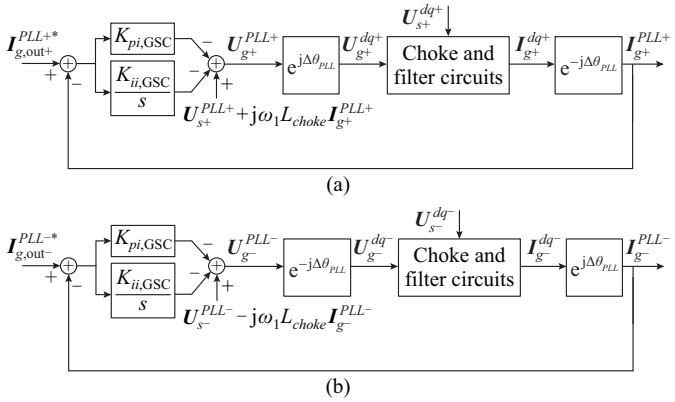

Fig. 9. Decoupled inner-loop control of GSC in PNSC-Tem. (a) Positive sequence. (b) Negative sequence.

IV. Detailed Sequence Current Analysis of BPSC

Based on the expressions of the DFIG in Section II and the space vector expressions of the BPSC in Section III, this section mathematically analyzes the positive- and negative-sequence current contributions of a DFIG-based WTG controlled with the BPSC strategy.

A. Positive-sequence Current Contribution

The reference tracking performance of the coupled inner-loop control of the BPSC is good [42]. Therefore, it is assumed that positive-sequence currents track the DC references in Fig. 4.

$$\begin{cases}\boldsymbol{I}_{r+}^{PLL+}=\boldsymbol{I}_{r,\mathrm{out}+}^{PLL+*}\\ \boldsymbol{I}_{g+}^{PLL+}=\boldsymbol{I}_{g,\mathrm{out}+}^{PLL+*}\end{cases} \tag{30}$$

Based on (14), the positive-sequence current contribution of the WTG is expressed as:

$$\boldsymbol{I}_{WTG+}^{PLL+}=\boldsymbol{I}_{s+}^{PLL+}+\boldsymbol{I}_{g+}^{PLL+}=\frac{U_{+}}{\mathrm{j}\omega_1 L_s}-\left(\frac{L_m}{L_s}\boldsymbol{I}_{r,\mathrm{out}+}^{PLL+*}-\boldsymbol{I}_{g,\mathrm{out}+}^{PLL+*}\right) \tag{31}$$

B. Negative-sequence Current Contribution

Based on Section III-A and Fig. 5(a), the negative-sequence rotor voltage introduced by the negative-sequence rotor current is expressed as:

$$\boldsymbol{U}_{r-}^{PLL+}=\mathrm{j}s\omega_1\boldsymbol{\psi}_{r-}^{PLL+}-K_{pi,\mathrm{RSC}}\boldsymbol{I}_{r-}^{PLL+}-K_{ii,\mathrm{RSC}}\int\boldsymbol{I}_{r-}^{PLL+}\mathrm{d}t \tag{32}$$

By substituting (19) into (32), it follows that:

$$\boldsymbol{U}_{r-}^{PLL+}=\mathrm{j}s\omega_1\boldsymbol{\psi}_{r-}^{dq-}\mathrm{e}^{-\mathrm{j}2\omega_1 t}\mathrm{e}^{-\mathrm{j}\theta_{U+}}-K_{pi,\mathrm{RSC}}\boldsymbol{I}_{r-}^{dq-}\mathrm{e}^{-\mathrm{j}2\omega_1 t}\mathrm{e}^{-\mathrm{j}\theta_{U+}}-\overbrace{K_{ii,\mathrm{RSC}}\mathrm{e}^{-\mathrm{j}\theta_{U+}}\int\boldsymbol{I}_{r-}^{dq-}\mathrm{e}^{-\mathrm{j}2\omega_1 t}\mathrm{d}t}^{\text{Integral term}} \tag{33}$$

Since the angular velocity of the disturbance signal is $2\omega_1$, the equivalent gain of the integrator is negligible ($K_{ii,\mathrm{RSC}}/2\omega_1$). So, the integral term in (33) is neglected. According to (19), the negative-sequence rotor voltage vector in the $dq-$ frame is expressed as:

$$\boldsymbol{U}_{r-}^{dq-}=\mathrm{j}s\omega_1\boldsymbol{\psi}_{r-}^{dq-}-K_{pi,\mathrm{RSC}}\boldsymbol{I}_{r-}^{dq-} \tag{34}$$

By substituting (34) into (16), the negative-sequence equivalent circuit of the DFIG under the BPSC is obtained as in Fig. 10, and the negative-sequence stator current is solved by:

$$\boldsymbol{I}_{s-}^{dq-}=\frac{\boldsymbol{U}_{s-}^{dq-}}{Z_{DFIG-}} \tag{35}$$

where Z_{DFIG-} is defined as the negative-sequence equivalent impedance of the DFIG under the BPSC and given by:

$$\begin{cases}Z_{DFIG-}=-\mathrm{j}\omega_1 L_s\dfrac{K_{pi,\mathrm{RSC}}-\mathrm{j}2\omega_1\sigma L_r}{K_{pi,\mathrm{RSC}}-\mathrm{j}2\omega_1 L_r}\\ \sigma=1-\dfrac{L_m^2}{L_s L_r}\end{cases} \tag{36}$$

where $L_{ls}=L_s-L_m$, $L_{lr}=L_r-L_m$.

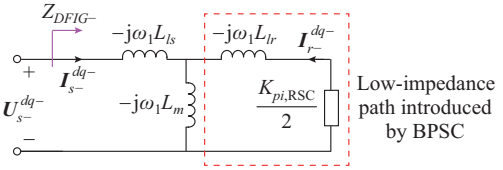

Fig. 10. Negative-sequence equivalent circuit of DFIG under BPSC.

Note that Z_{DFIG-} consists of not only a reactance (imaginary part) but also a resistance. As a result, the negative-sequence stator current includes both the I2A and I2R.

Similarly, the negative-sequence current of the GSC is:

$$\boldsymbol{I}_{g-}^{dq-}=\frac{\boldsymbol{U}_{s-}^{dq-}}{K_{pi,\mathrm{GSC}}} \tag{37}$$

So, the negative-sequence current contribution of the DFIG-based WTG under the BPSC strategy is:

$$\boldsymbol{I}_{WTG-}^{dq-}=\boldsymbol{I}_{s-}^{dq-}+\boldsymbol{I}_{g-}^{dq-}=\frac{\boldsymbol{U}_{s-}^{dq-}}{Z_{DFIG-}}+\frac{\boldsymbol{U}_{s-}^{dq-}}{K_{pi,\mathrm{GSC}}} \tag{38}$$

C. Current Capacity and Overcurrent Problem

The current capacity of RSC and GSC is determined by the switching device, typically the insulated gate bipolar transistor (IGBT). It withstands up to 200% of its rated current but only for a very short period (typically no more than 10 ms). It can continuously withstand 120% of its rated current [43].

In the BPSC strategy, almost all the current capacity of RSC is assigned to positive-sequence currents. As a result, when there are negative-sequence components circulating in the rotor winding, the rotor current will easily exceed 1.2 p.u..

According to Fig. 10 and (36), the negative-sequence rotor current is given as:

$$\boldsymbol{I}_{r-}^{dq-}=\frac{\mathrm{j}\omega_1 L_m}{-\mathrm{j}\omega_1 L_r+K_{pi,\mathrm{RSC}}/2}\boldsymbol{I}_{s-}^{dq-}=\frac{L_m}{L_s}\frac{\boldsymbol{U}_{s-}^{dq-}}{\mathrm{j}\omega_1\sigma L_r-K_{pi,\mathrm{RSC}}/2} \tag{39}$$

Consider the practical parameters of a 1.5 MW DFIG-based WTG given in Table I. By employing these parameters into (36) and (39), Z_{DFIG-} and the negative-sequence rotor current are numerically calculated for this particular DFIG as:

$$\begin{cases} Z_{DFIG-}=0.380+\mathrm{j}0.362 \\ \boldsymbol{I}_{r-}^{dq-}=\dfrac{\boldsymbol{U}_{s-}^{dq-}}{0.5586\mathrm{e}^{\mathrm{j}2.4647}} \end{cases} \tag{40}$$

TABLE I
PARAMETERS OF 1.5 MW DFIG-BASED WTG

Parameter	Value	Parameter	Value
U_B	469.485 V	$I_{\mathrm{RSC,max}}$	1.2 p.u.
Rated active power	1.5 MW	$I_{\mathrm{GSC,max}}$	0.36 p.u.
S_B	1.667 MVA	$K_{pi,\mathrm{RSC}}$	0.82
R_s	0.033 p.u.	$K_{ii,\mathrm{RSC}}$	12.13
R_r	0.026 p.u.	$K_{pi,\mathrm{GSC}}$	5
ω_1	120π rad/s	$K_{ii,\mathrm{GSC}}$	98
s	−0.2	K_{V+}	2
$\omega_1 L_s$	3.08 p.u.	K_{V-}	2
$\omega_1 L_r$	3.06 p.u.	$K_{p,PLL}$	100
$\omega_1 L_m$	2.9 p.u.	$K_{i,PLL}$	1250
DC voltage U_{DC}^*	1150 V	N_r/N_s	3:1

This indicates that, under the BPSC, the coupled inner-loop control introduces a low-impedance path through rotor winding (see Fig. 10). As a result, Z_{DFIG-} is much smaller than the magnetizing impedance and the negative-sequence rotor current is significant. For instance, when the negative-sequence voltage is 0.217 p.u., the magnitude of negative-sequence rotor current will be 0.388 p.u., and the rotor current will easily go over 1.2 p.u.. In practice, the overcurrent protection will be triggered to bypass the RSC with crowbar. Therefore, it is unpractical to expect that the BPSC strategy would meet I2R requirements.

V. DETAILED SEQUENCE CURRENT ANALYSIS OF PNSC-TEM AND EXISTING COORDINATED CONTROL

Based on the DFIG equations in Section II and the space vector formulations in Section III, this section theoretically analyzes the positive- and negative-sequence current contributions of a DFIG-based WTG controlled with the PNSC-Tem and the existing coordinated control.

A. Positive-sequence Current Contribution

The positive-sequence current contribution of a DFIG-based WTG under the PNSC-Tem has the same form in (31).

B. Negative-sequence Current Contribution

The PNSC-Tem and the existing coordinated control have independent RSC inner-loop controllers to regulate the negative-sequence rotor currents, as shown in Fig. 8. The references can be achieved without steady-state error, so we have:

$$\boldsymbol{I}_{r-}^{PLL-}=\boldsymbol{I}_{r,\mathrm{out}-}^{PLL-*} \tag{41}$$

Based on (16), the negative-sequence current of DFIG is:

$$\boldsymbol{I}_{WTG-}^{PLL-}=\frac{\boldsymbol{U}_{s-}^{PLL-}}{-\mathrm{j}\omega_1 L_s}-\frac{L_m}{L_s}\boldsymbol{I}_{r,\mathrm{out}-}^{PLL-*}+\boldsymbol{I}_{g,\mathrm{out}-}^{PLL-*} \tag{42}$$

where the negative-sequence current of GSC should be accounted when the existing coordinated control is employed.

C. I2R Direction Problem

By substituting (26) into (42), we have:

$$\boldsymbol{I}_{WTG-}^{PLL-}=\frac{\boldsymbol{U}_{s-}^{PLL-}}{-\mathrm{j}\omega_1 L_s}-\frac{L_m}{L_s}\frac{\boldsymbol{U}_{s-}^{PLL-}}{U_+}\bar{\boldsymbol{I}}_{r,\mathrm{out}+}^{PLL+*}+\boldsymbol{I}_{g,\mathrm{out}-}^{PLL-*} \tag{43}$$

Note that, the d-axis component of $\boldsymbol{I}_{WTG-}^{PLL-}$ does not correspond to I2A since $PLL-$ is not aligned with the negative sequence voltage vector. Similarly, its q-axis component does not correspond to I2R. The negative-sequence voltage reference frame $SVR-$ needs to be introduced to align these components with I2A and I2R.

In steady state, the transformation from $PLL-$ to $SVR-$ frames is:

$$\boldsymbol{X}_{-}^{SVR-}=\boldsymbol{X}_{-}^{PLL-}\mathrm{e}^{-\mathrm{j}\theta_{V-}}=\boldsymbol{X}_{-}^{PLL-}\mathrm{e}^{-\mathrm{j}(\theta_{U+}-\theta_{-})} \tag{44}$$

where θ_{V-} is from the DDSRF-PLL in Fig. 6.

By substituting (44) into (26), the negative-sequence rotor current in $SVR-$ is expressed as:

$$\boldsymbol{I}_{r-}^{SVR-*}=\frac{U_-}{U_+}\bar{\boldsymbol{I}}_{r+}^{PLL+*}\Rightarrow I_{rq-}^{SVR-*}=-\frac{U_-}{U_+}I_{rq+}^{PLL+*} \tag{45}$$

By substituting (45) into (43), the I2R contributed by WTG is expressed as:

$$I_{WTGq-}^{SVR-}=\frac{U_-}{\omega_1 L_s}+\frac{L_m}{L_s}\frac{U_-}{U_+}I_{rq,\mathrm{out}+}^{PLL+*}+I_{gq,\mathrm{out}-}^{SVR-*} \tag{46}$$

During FRT, $I_{rq,\mathrm{out}+}^{PLL+*}$ will be negative to provide the required I1R from the stator side (see (24)). As a result, the second term of (46) is also negative, which will increase the negative-sequence voltage level and voltage unbalance because the required I2R is positive as shown in Fig. 1. This would be in violation of I2R requirements in the emerging grid codes.

Since the existing coordinated control and PNSC-Tem have the same RSC negative-sequence control, the I2R contributed by stator is also negative. Although the GSC negative-sequence control is designed to provide positive I2R, according to (46), the I2R contributed by the WTG cannot reach the required value.

D. RSC Over-modulation Problem

According to the steady-state relationship in Section II, the rotor voltage demand of the RSC control can be expressed as:

$$U_{r,demand}=\left|\boldsymbol{U}_{r+}^{PLL+}\right|+\left|\boldsymbol{U}_{r-}^{SVR-}\right| \tag{47}$$

$$\boldsymbol{U}_{r+}^{PLL+}\approx s\left(\mathrm{j}\omega_1\sigma L_r\boldsymbol{I}_{r,\mathrm{out}+}^{PLL+*}+\frac{L_m}{L_s}U_+\right) \tag{48}$$

$$\boldsymbol{U}_{r-}^{SVR-}\approx(2-s)\left(-\mathrm{j}\omega_1\sigma L_r\boldsymbol{I}_{r,\mathrm{out}-}^{SVR-}+\frac{L_m}{L_s}U_-\right) \tag{49}$$

Since the PNSC-Tem and the existing coordinated control have the same RSC control, they have the same rotor voltage demand. By substituting (45) into (49) and considering that $\boldsymbol{I}_{rq,\mathrm{out}+}^{PLL+*}$ is dominated during FRT, (49) can be simplified as:

$$\boldsymbol{U}_{r-}^{SVR-}\approx(2-s)\left(-\omega_1\sigma L_r\frac{U_-}{U_+}I_{rq+}^{PLL+*}+\frac{L_m}{L_s}U_-\right) \tag{50}$$

Since $I_{rq\_\mathrm{out}+}^{PLL+*}$ is negative during FRT, the control target of eliminating the oscillation of Tem increases the rotor voltage demand. As a result, under the PNSC-Tem and the existing coordinated control, the RSC is more likely to be over-modulated under voltage imbalance. Considering the two-level VSC and the space vector modulation, the RSC voltage capacity seen from the stator winding in per unit should satisfy:

$$U_{r,demand}<\frac{4}{\pi}\frac{U_{DC}^*}{U_B\sqrt{3}}\frac{1}{N_r/N_s} \tag{51}$$

When the rotor voltage demanded by the decoupled inner-loop controller is greater than the maximum value in (51), the RSC cannot achieve the rotor voltage references and the rotor current is out of control. As a result, the overcurrent protection will be triggered again.

VI. The Proposed Coordinated Control

The analysis in Sections IV and V shows that the existing control solutions (BPSC, PNSC-Tem, and the existing coordinated control) cannot comply with I2R requirements under severe voltage unbalance following asymmetrical faults at the grid side. To overcome this challenge, this section proposes a new coordinated control strategy (PNSC-I12R) for the DFIG converters.

A. Current Reference Generation and Allocation

First, the new proposed strategy needs to comply with the I1R requirements, and the positive-sequence current references in Section III-A are adopted.

According to [11], the required I2R can be expressed as:

$$I_{WTGq-}^{SVR-}=K_{V\_}U_- \tag{52}$$

By substituting (52) into (16), the rotor current reference before the limiter is expressed as:

$$I_{rq,\mathrm{in}-}^{SVR-*}=\left(\frac{1}{\omega_1 L_m}-\frac{L_sK_{V\_}}{L_m}\right)U_- \tag{53}$$

When the RSC current capacity is not sufficient, the limiter will function. The negative-sequence stator current taking the reference current after the limiter is given by:

$$I_{sq-}^{SVR-}=-\frac{L_m}{L_s}I_{rq,\mathrm{out}-}^{SVR-*}+\frac{U_-}{\omega_1 L_s} \tag{54}$$

The rest of I2R will be contributed by GSC, and the I2R current reference before the limiter is:

$$I_{gq,\mathrm{in}-}^{SVR-*}=K_{V\_}U_--I_{sq-}^{SVR-}=K_{V\_}U_-+\frac{L_m}{L_s}I_{rq,\mathrm{out}-}^{SVR-*}-\frac{U_-}{\omega_1 L_s} \tag{55}$$

I2A is set to be 0 to spare the current capacity of converters.

B. Priority Level Setting

To avoid overcurrent and meet I1R and I2R requirements, the priority levels are set as shown in Fig. 11.

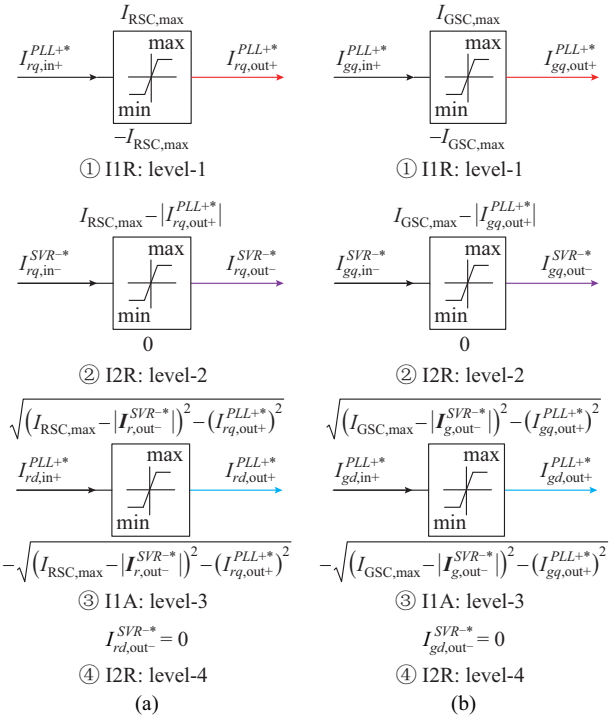

Fig. 11. Limiter and priority settings in proposed control strategy PNSC-I12R. (a) RSC. (b) GSC.

C. PNSC-I12R

A schematic of the PNSC-I12R is shown in Fig. 12. Firstly, the control is built on the positive-sequence voltage orientation that is achieved by DDSRF-PLL. Secondly, the three-phase measurements are decomposed into positive- and negative-sequence vectors. Thirdly, eight different current references are generated according to Section VI-A to provide the required I1R and I2R. Fourthly, the priority level settings in Fig. 11 are used to coordinate the current references to avoid overcurrent. Finally, eight inner-loop controllers are employed to achieve the current references of the RSC and GSC.

D. Advantage of the Proposed Control Strategy

Since $I_{rd,\mathrm{out}-}^{SVR-*}$ is set to zero, the negative-sequence rotor voltage in (49) becomes:

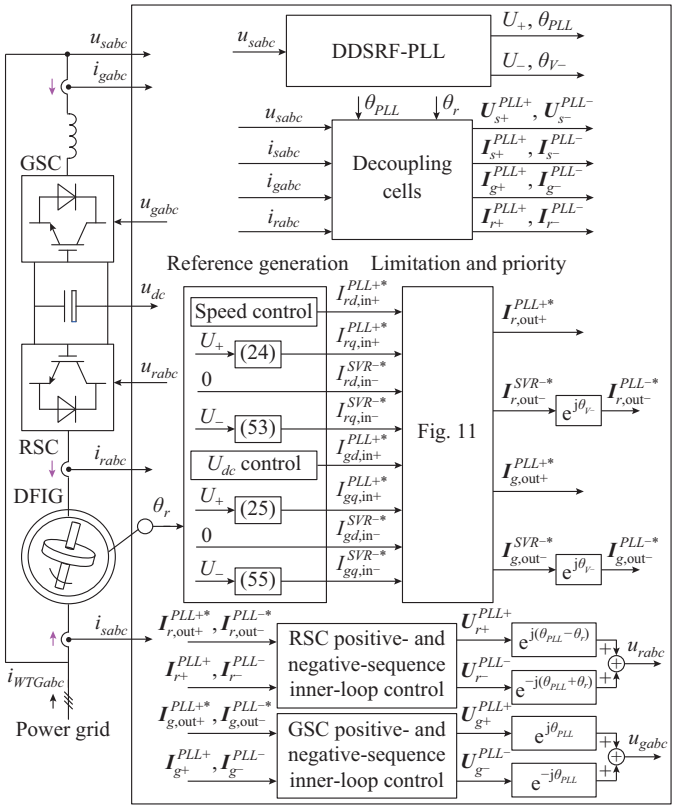

Fig. 12. Schematic of the proposed coordinated control strategy PNSC-I12R.

$$\boldsymbol{U}_{r-}^{SVR-} \cong (2-s)\left(\omega_1 \sigma L_r I_{rq-}^{SVR-} + \frac{L_m}{L_s} U_-\right) \tag{56}$$

Under the PNSC-I12R scheme, $I_{rq,\,\mathrm{out}-}^{SVR-*}$ is negative to provide the required I2R (as shown in (53)). As a result, the rotor voltage demand of the PNSC-I12R is smaller than that of the PNSC-Tem and the existing coordinated control. It enables the DFIG-based WTG to provide the required I1R and I2R within the current and voltage capacities of converters under severe voltage unbalances following asymmetrical short circuits.

VII. Validation and Comparisons

This section validates the prior mathematical investigations and the proposed control strategy with EMT simulations. The performances of DFIG-based WTG under the BPSC, existing coordinated control, and PNSC-I12R are compared.

A. Electric Power Research Institute (EPRI) Benchmark System and Fault Scenario

The 120 kV 60 Hz EPRI benchmark system in Fig. 13 is used as the test system. A double line-to-ground fault (ABG) is applied at Bus 3 for a duration of one second. A WP, consisting of 45×1.5 MW DFIG-based WTGs, is operating at the rated active power before the fault inception. The parameters of the DFIG-based WTG are listed in Table I. Reference [17] details the WP and EPRI benchmark system. Note that, in EMT simulations, the overcurrent protection is disabled, and the voltage constraint of the RSC is blocked to present the voltage and current demands of different control strategies. In practice, once the rotor current or the rotor voltage demand exceeds the capacity, the crowbar circuit is triggered, and the DFIG-based WTG would fail to comply with the emerging grid codes.

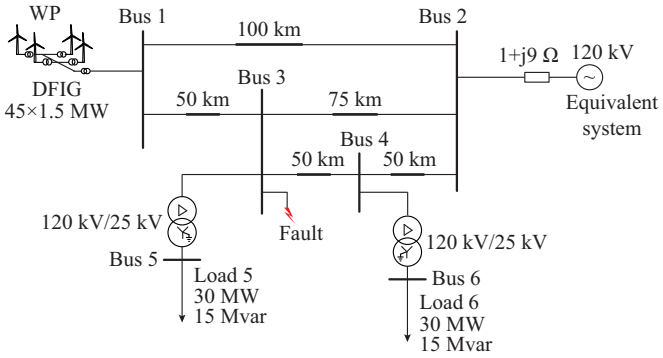

Fig. 13. Single-line diagram of 120 kV 60 Hz EPRI benchmark system.

B. DFIG-based WTG under BPSC

The simulation results of the DFIG under the BPSC strategy are shown in the left column of Fig. 14. As shown in Fig. 14(d), the current capacity is primarily assigned to I1R. Then, the remaining current capacity is assigned to I1A. Moreover, as shown in Fig. 14(e), the I2A and I2R components are significant which suggests that DFIG can be represented with a low impedance in the negative-sequence system. This will result in rotor current exceeding the RSC current capacity (1.2 p.u.) as shown in Fig. 14(g). These simulation results support the RSC overcurrent problem analyzed in Section IV-C and validates the maximum continuous current estimated by (40). Despite the overcurrent, I2R is not sufficient to meet the requirements in the German grid code. Also the significant oscillations on the Tem shown in Fig. 14(f) should be noted.

C. DFIG-based WTG Under the Existing Coordinated Control

The difference between the PNSC-Tem and the existing coordinated control is on the negative-sequence control of the GSC. The existing coordinated control [28] contributes I2R through the GSC and it is one step forward in meeting grid code requirements on I2R compared with the PNSC-Tem. Therefore, the PNSC-Tem is discarded from comparisons. The simulation results of the DFIG controlled with the existing coordinated control are shown in the middle column of Fig. 14. As shown in Fig. 14(d), the remaining current capacity of the RSC, apart from the I1R, is assigned to the negative-sequence current based on (26). As a result, the oscillations in Tem are effectively eliminated as shown in Fig. 14(f). However, as shown in Fig. 15 and Fig. 14(c), the consequent stator I2R is negative. Even though the GSC provides positive I2R according to (29), the resultant I2R is still insufficient. Moreover, as shown in Fig. 14(h), the rotor voltage demand is greater than the maximum value. It means that the RSC is over-modulated under this practical asymmetrical short circuit. In practice, the crowbar needs to be activated to deal with the over-modulation and overcurrent. The simulation results validate the difficulties analyzed in Section V-C and Section V-D.

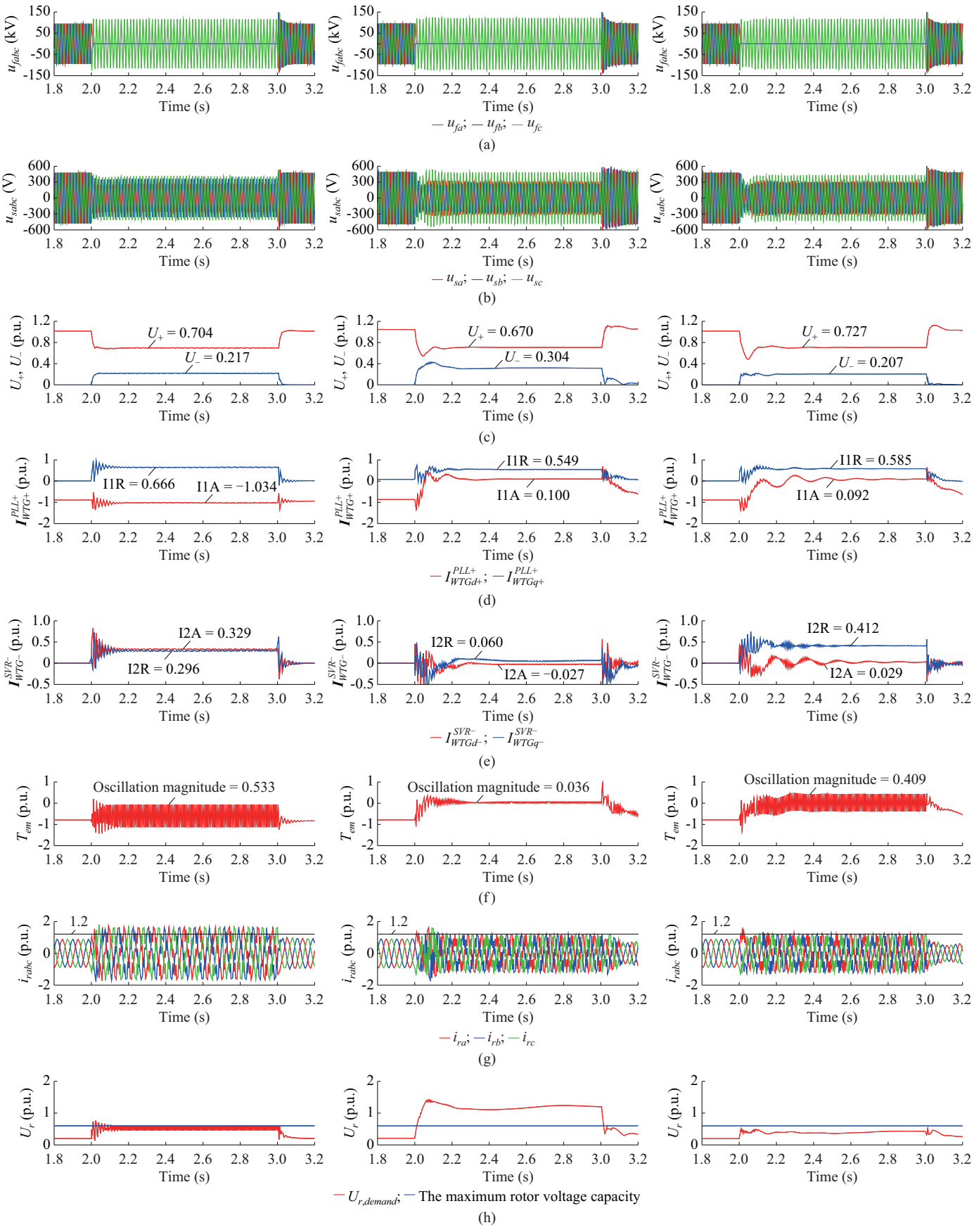

Fig. 14. Simulation results of DFIG-based WTG under three different control strategies. (a) Three-phase voltage at faulted bus. (b) Three-phase stator voltage. (c) Magnitudes of positive- and negative-sequence stator voltage vectors. (d) Positive-sequence active and reactive currents. (e) Negative-sequence active and reactive currents. (f) Tem. (g) Three-phase rotor current and limit. (h) Rotor voltage demand and limit.

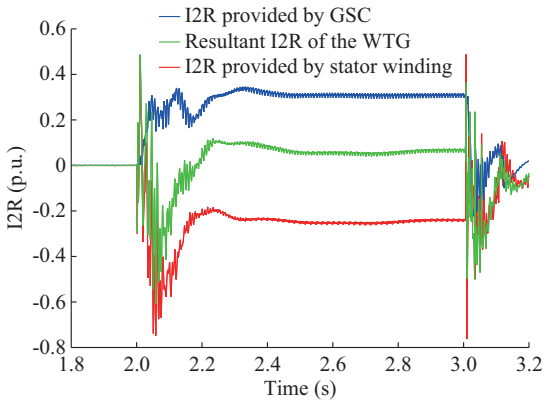

Fig. 15. Resultant I2R and its components under the existing coordinated control.

D. DFIG-based WTG Under New PNSC-I12R

The simulation results of the DFIG under the PNSC-I12R are shown in the right column of Fig. 14. As shown in Fig. 14(d), the remaining RSC current capacity, apart from I1R, is assigned to the required I2R which is positive as shown in (52) and Fig. 14(e). As a result, the negative-sequence voltage and overvoltage on the healthy phase are suppressed as shown in Fig. 14(a) and (c). I2R is in line with the setting of its gain. As shown in Fig. 14(f), although the oscillations in torque still exists, its amplitude is smaller than that under the BPSC.

Moreover, as shown in Fig. 14(g) and (h), the rotor current and the rotor voltage demand both have the maximum values. It means that the proposed PNSC-I12R scheme can normally operate and contribute I1R and I2R under this practical double-line-to-ground short circuit.

E. Comparisons

In terms of I1R, all the three control strategies have similar performances that comply with the requirement in (23), as shown in Fig. 14(d).

In terms of I2R, the BPSC and the existing coordinated control cannot meet the requirement in (52) as shown in Fig. 14(e). More specifically, the BPSC fails to comply with the I2R requirement because of the RSC overcurrent problem. The existing coordinated control fails to comply with the I2R requirement because of the RSC over-modulation and the I2R direction problems. As shown in Fig. 14(a) and (b), under the new proposed PNSC-I12R, the required I2R is successfully achieved. Moreover, the demands of the rotor voltage and rotor current are all within the capacity.

VIII. Conclusion

In some recent grid codes, WTGs are not only required to provide I1R but also I2R. This paper first investigates the I2R characteristics of DFIG-based WTGs under existing control strategies, namely the BPSC, PNSC-Tem, and an existing coordinated control. Both the mathematical analysis and simulations show that these control strategies fail to comply with the requirements on I2R under severe voltage unbalance due to asymmetrical faults. Then, this paper proposes a new coordinated control strategy denoted by PNSC-I12R to solve this shortcoming of the existing control schemes.

The performances of the above control strategies are summarized as follows.

1) Under the conventional BPSC strategy, almost all the current capacity of RSC is allocated to the positive-sequence currents. Moreover, the coupled inner-loop control of RSC introduces a low-impedance path through the rotor winding with a resistive component. Consequently, the DFIG contributes not only I2R but also I2A to the grid, and the negative-sequence rotor current is also significant. The I2A and I2R components can be simply predicted with the proposed negative-sequence equivalent impedance Z_{DFIG-} in (38). Under practical voltage unbalance due to asymmetrical faults, the rotor current would easily exceed the current capacity of the RSC (1.2 p.u.) and trigger overcurrent and crowbar protections.

2) Under the PNSC-Tem and the existing coordinated control, after fulfilling the I1R requirement, the rest of the RSC current capacity is allocated to the negative-sequence current to eliminate the double grid frequency oscillations in Tem. However, from the grid perspective, the elimination of the double grid frequency oscillations is achieved at the expense of producing an I2R that is the opposite of what is required. As a result, under practical voltage unbalance following asymmetrical short circuits, even though the existing coordinated control provides a positive I2R through the GSC, the resultant I2R is still insufficient. It cannot help suppress overvoltages on healthy phases. On the contrary, it aggravates the overvoltage problem under unbalanced fault conditions. Moreover, under these control strategies, the rotor voltage demand of the RSC control can easily exceed the maximal value. It will result in RSC over-modulation and make the rotor current out of control.

3) The proposed coordinated control strategy, i.e., PNSC-I12R, primarily allocates the current capacity to the I1R and I2R components. The DDSRF-PLL provides the reference frames ($PLL+$ and $SVR-$) for the evaluation of the active and reactive components in the positive- and negative-sequence systems. Then, eight different current references are calculated according to the proposed expressions. On one hand, the control target is proven to effectively reduce the rotor voltage demand of the RSC control. On the other hand, this strategy reduces the negative-sequence and healthy phase voltages at the grid side effectively by making full use of the current and voltage capacities of the converters. These advantages make the proposed control strategy become a better solution for practical voltage unbalances due to asymmetrical faults. In addition, the amplitude of the oscillations in Tem is also less compared with the BPSC.

Considering the proposed control strategy and the analytical investigations in this paper, future work and applications include: ① developing sequence-domain circuit models of DFIG-based WTGs and WPs by considering various types of control strategies and grid codes for practical short circuit studies; ② investigating the impact of different control strategies on protection elements such as negative sequence-based elements including the differential protection element based on the alpha plane and fault identification element.

REFERENCES

[1] P. E. Sutherland, "Ensuring stable operation with grid codes: a look at Canadian wind farm interconnections," *IEEE Industry Applications Magazine*, vol. 22, no. 1, pp. 60-67, Jan.-Feb. 2016.

[2] R. Teodorescu, M. Liserre, and P. Rodríguez, "Grid requirements for WT systems," in *Grid Converters for Photovoltaic and Wind Power Systems*. New Delhi: IEEE Press, 2011, pp. 145-167.

[3] IRENA. (2016, May). Scaling up variable renewable power: the role of grid codes. [Online]. Available: http://environmentportal. in/content/428960/scaling-up-variable-renewable-power-the-role-of-grid-codes/

[4] I. Machado, "Grid codes comparison," M. S. thesis, Department of Electric Power Engineering, Chalmers University of Technology, Göteborg, Sweden, 2006.

[5] FERC. (2005, Dec.). Interconnection for wind energy. [Online]. Available: https://www. ferc. gov/sites/default/files/2020-05/20051212171744-RM05-4-001.pdf

[6] ENTSO-E. (2007, Jan.). Nordic grid code 2007–Nordic collection of rules, 2007. [Online]. Available: https://eepublicdownloads. entsoe. eu/clean-documents/pre2015/publications/nordic/planning/070115_entsoe_nordic_NordicGridCode.pdf

[7] E. ON. (2006, Apr.). Grid code–high and extra high voltage. [Online]. Available: http://www. pvupscale. org/IMG/pdf/D4_2_DE_annex_A-3_EON_HV_grid_connection_requirements_ENENARHS2006de.pdf

[8] *Technical Rule for Connecting Wind Farm to Power System*, GB/T 19963-2011, 2011.

[9] C. Shen, Z. Shuai, Y. Shen *et al.*, "Transient stability and current injection design of paralleled current-controlled VSCs and virtual synchronous generators," *IEEE Transactions on Smart Grid*, vol. 12, no. 2, pp. 1118-1134, Mar. 2021.

[10] M. V. A. Nunes, J. A. P. Lopes, H. H. Zurn *et al*., "Influence of the variable-speed wind generators in transient stability margin of the conventional generators integrated in electrical grids," *IEEE Transactions on Energy Conversion*, vol. 19, no. 4, pp. 692-701, Dec. 2004.

[11] VDE. (2018, Oct.). VDE-AR-N 4120: technical connection rules for high-voltage. [Online]. Available: https://www. vde. com/en/fnn/topics/technical-connection-rules/tar-for-high-voltage

[12] VDE. (2018, Oct.). Technical requirements for the connection and operation of customer installations to the medium-voltage network (TCC medium-voltage). [Online]. Available: https://www.vde.com/en/fnn/topics/technical-connection-rules/tcr-for-medium-voltage

[13] *Technical Specification for Connecting Wind Farm to Power System–Part 1: Onshore Wind Power*, GB/T 19963.1-2021, 2021.

[14] V. Diedrichs, H. Lorenzen, I. Mackensen *et al*., "Asymmetrical current injection addressed by ENTSO-E draft network code–requirements & development of technology for wEC," in *Proceedings of the 11th Wind Integration Workshop*, Lisbon, Portugal, Nov. 2012, pp. 1-7.

[15] A. Haddadi, M. Zhao, I. Kocar *et al*., "Impact of inverter-based resources on negative sequence quantities-based protection elements," *IEEE Transactions on Power Delivery*, vol. 36, no. 1, pp. 289-298, Feb. 2021.

[16] A. Haddadi, I. Kocar, J. Mahseredjian *et al*., "Performance of phase comparison line protection under inverter-based resources and impact of the German grid code," in *Proceedings of 2020 IEEE Power & Energy Society General Meeting (PESGM)*, Montreal, Canada, Aug. 2020, pp. 1-5.

[17] EPRI, "Impact of renewables on system protection: wind/PV Short-circuit phasor model library and guidelines for system protection studies," Palo Alt, Tech. Rep. 3002002810, Nov. 2014.

[18] B. Wang and L. Jing, "A protection method for inverter-based microgrid using current-only polarity comparison," *Journal of Modern Power Systems and Clean Energy*, vol. 8, no. 3, pp. 446-453, May 2020.

[19] D. Xiang, L. Ran, P. J. Tavner *et al*., "Control of a doubly fed induction generator in a wind turbine during grid fault ride-through," *IEEE Transactions on Energy Conversion*, vol. 21, no. 3, pp. 652-662, Sept. 2006.

[20] L. Chen, B. Zhang, and X. Fan, "Asymmetrical fault ride-through control strategy for rotor-side converter of DFIG," *IEEE Transactions on Energy Conversion*, vol. 35, no. 2, pp. 1046-1053, Jun. 2020.

[21] D. Zhu, X. Zou, L. Deng *et al*., "Inductance-emulating control for DFIG-based wind turbine to ride-through grid faults," *IEEE Transactions on Power Electronics*, vol. 32, no. 11, pp. 8514-8525, Nov. 2017.

[22] H. Xu, X. Ma, and D. Sun, "Reactive current assignment and control for DFIG based wind turbines during grid voltage sag and swell conditions," *Journal of Power Electronics*, vol. 15, no. 1, pp. 235-245, Jan. 2015.

[23] L. Xu, "Enhanced control and operation of DFIG-based wind farms during network unbalance," *IEEE Transactions on Energy Conversion*, vol. 23, no. 4, pp. 1073-1081, Dec. 2008.

[24] J. Hu, H. Xu, and Y. He, "Coordinated control of DFIG's RSC and GSC under generalized unbalanced and distorted grid voltage conditions," *IEEE Transactions on Industrial Electronics*, vol. 60, no. 7, pp. 2808-2819, Jul. 2013.

[25] U. Karaagac, J. Mahseredjian, R. Gagnon *et al*., "A generic EMT-type model for wind parks with permanent magnet synchronous generator full size converter wind turbines," *IEEE Power and Energy Technology Systems Journal*, vol. 6, no. 3, pp. 131-141, Sept. 2019.

[26] M. G. Taul, X. Wang, P. Davari *et al*., "Current reference generation based on next-generation grid code requirements of grid-tied converters during asymmetrical faults," *IEEE Journal of Emerging and Selected Topics in Power Electronics*, vol. 8, no. 4, pp. 3784-3797, Dec. 2020.

[27] T. Neumann, T. Wijnhoven, G. Deconinck *et al*., "Enhanced dynamic voltage control of type 4 wind turbines during unbalanced grid faults," *IEEE Transactions on Energy Conversion*, vol. 30, no. 4, pp. 1650-1659, Dec. 2015.

[28] H. Xu, Y. Zhang, Z. Li *et al*., "Reactive current constraints and coordinated control of DFIG's RSC and GSC during asymmetric grid condition," *IEEE Access*, vol. 8, pp. 184339-184349, Oct. 2020.

[29] *Short-circuit Currents in Three-phase A.C. Systems–Part 0: Calculation of Currents*, IEC 60909-0: 2016, 2016.

[30] F. Sulla, J. Svensson, and O. Samuelsson, "Symmetrical and unsymmetrical short-circuit current of squirrel-cage and doubly-fed induction generators," *Electric Power Systems Research*, vol. 81, pp. 1610-1618, Apr. 2011.

[31] G. Pannell, D. J. Atkinson, and B. Zahawi, "Analytical study of grid-fault response of wind turbine doubly fed induction generator," *IEEE Transactions on Energy Conversion*, vol. 25, no. 4, pp. 1081-1091, Dec. 2010.

[32] Y. Chang, J. Hu, and X. Yuan, "Mechanism analysis of DFIG-based wind turbine's fault current during LVRT with equivalent inductances," *IEEE Journal of Emerging and Selected Topics in Power Electronics*, vol. 8, no. 2, pp. 1515-1527, Jun. 2020.

[33] L. V. Strezoski, N. R. Vojnovic, V. C. Strezoski *et al*., "Modeling challenges and potential solutions for integration of emerging DERs in DMS applications: power flow and short-circuit analysis," *Journal of Modern Power Systems and Clean Energy*, vol. 7, no. 6, pp. 1365-1384, Nov. 2019.

[34] G. Abad, J. Lopez, M. A. Rodriguez *et al*., "Steady state of the doubly fed induction machine," in *Doubly Fed Induction Machine: Modeling and Control for Wind Energy Generation Applications*. Hoboken: Wiley-IEEE Press, 2011, pp. 155-208.

[35] S. Engelhardt, J. Kretschmann, J. Fortmann *et al*., "Capability and limitations of DFIG based wind turbines concerning negative sequence control," in *Proceedings of 2013 IEEE PES General Meeting*, Vancouver, Canada, Jul. 2013, pp. 1-5.

[36] J. Pyrhonen, V. Hrabovcová, and S. R. Semken, "Fundamentals of space-vector theory," in *Electrical Machine Drives Control: An Introduction*. Chicherster: Wiley-IEEE Press, 2016, pp. 66-90.

[37] L. Xu and Y. Wang, "Dynamic modeling and control of DFIG-based wind turbines under unbalanced network conditions," *IEEE Transactions on Power Systems*, vol. 22, no. 1, pp. 314-323, Feb. 2007.

[38] G. O. Calabrese, "The mathematical theory of symmetrical components for three-phase circuits," in *Symmetrical Components Applied to Electric Power Networks*. New York: Ronald Press, 1959, pp. 114-141.

[39] R. Teodorescu, M. Liserre, and P. Rodriguez, "Grid converter control for WTS," in *Grid Converters for Photovoltaic and Wind Power Systems*. New Delhi, India: IEEE Press, 2007, pp. 205-236.

[40] G. Abad, J. Lopez, M. A. Rodriguez *et al*., "Vector control strategies for grid-connected DFIM wind turbines," in *Doubly Fed Induction Machine: Modeling and Control for Wind Energy Generation Applications*. Hoboken, New Jersey: Wiley-IEEE Press, 2011, pp. 327-328.

[41] U. Subudhi, H. K. Sahoo, and S. K. Mishra, "Adaptive three-phase estimation of sequence components and frequency using H_∞ filter based on sparse model," *Journal of Modern Power Systems and Clean Energy*, vol. 8, no. 5, pp. 981-990, Sept. 2020.

[42] Y. Chang and J. Hu, "Modeling, analysis and parameters design of rotor current control in DFIG-based wind turbines for dynamic performance optimizing," in *Proceedings of 2017 IEEE Energy Conversion Congress and Exposition (ECCE)*, Cincinnati, USA, Oct. 2017, pp. 3303-3308.

[43] N. Mohan, T. M. Undeland, and W. Robbins, *Power Electronics: Converters, Applications and Design*. New York: Wiley, 2003, pp. 626-637, 208-210.

Yuanzhu Chang received the B.Eng. and Ph.D. degrees in electrical engineering from the School of Electrical and Electronic Engineering, Huazhong University of Science and Technology, Wuhan, China, in 2014 and 2020, respectively. He is currently working as a Postdoctoral Fellow at Polytechnique Montréal, University of Montréal, Montréal, Canada. His research interests include fault ride through control, fault analysis, and protection relay of power systems.

Ilhan Kocar received the B.Sc. and M.Sc. degrees in electrical and electronics engineering from Orta Doğu Teknik Üniversitesi, Ankara, Turkey, in 1998 and 2003, respectively, and the Ph.D. degree in electrical engineering from Polytechnique/Université de Montréal, Montréal, Canada, in 2009. He worked as a Project Engineer at Aselsan Electronics Inc., Ankara, Turkey, between 1998 and 2004. He worked as a Distribution Software R&D Engineer at CYME International T&D, St-Bruno, Canada, between 2009 and 2011. He joined the Faculty at Polytechnique Montréal in 2011. His career highlights include major contributions to professional simulation tools, and development of solutions for large-scale integration of inverter-based resources (IBRs). His research interests include design, rigorous mathematical modeling, analysis, and validation of field measurements.

Jiabing Hu received the B.Eng. and Ph.D. degrees both in electrical engineering from the College of Electrical Engineering, Zhejiang University, Hangzhou, China, in 2004 and 2009, respectively. From April 2010 to August 2011, he was a Postdoctoral Research Associate with Sheffield Siemens Wind Power (S2WP) Research Center and the Department of Electronic and Electrical Engineering, University of Sheffield, Sheffield, U.K.. Since September 2011, he has been a Professor in the State Key Laboratory of Advanced Electromagnetic Engineering and Technology, School of Electrical and Electronic Engineering, Huazhong University of Science and Technology, Wuhan, China. His current research interests include grid-integration of large-scale renewables, modular multilevel converter for high-voltage direct current (HVDC) applications, and modeling, analysis, and control of power electronized power systems.

Ulas Karaagac received the B.Sc. and M.Sc. degrees in electrical and electronics engineering from the Middle East Technical University, Ankara, Turkey, in 1999 and 2002, respectively, and the Ph.D. degree in electrical engineering from Polytechnique Montréal, Montréal, Canada, in 2011. He was a Research and Development Engineer with the Information Technology and Electronics Research Institute (BILTEN), Scientific and Technical Research Council of Turkey (TUBITAK), Ankara, Turkey, from 1999 to 2007. He was also a Postdoctoral Fellow with Polytechnique Montréal, from 2011 to 2013, and a Research Associate, from 2013 to 2016. In 2017, he joined the Department of Electrical Engineering, The Hong Kong Polytechnic University, Hong Kong, China, where he is currently an Assistant Professor. His research interests include integration of large-scale renewables into power grids, modeling and simulation of large-scale power systems, and power system dynamics and control.

Ka Wing Chan received the B.Sc. (Hons) and Ph.D. degrees in electronic and electrical engineering from the University of Bath, Bath, U.K., in 1988 and 1992, respectively. He currently is an Associate Professor and Associate Head in the Department of Electrical Engineering of the Hong Kong Polytechnic University, Hong Kong, China. His research interests include power system stability, analysis and control, power grid integration, security, resilience and optimization, demand response management, etc.

Jean Mahseredjian received the Ph.D. degree in electrical engineering from Polytechnique Montréal, Montréal, Canada, in 1991. From 1987 to 2004, he was with IREQ (Hydro-Quebec), Montréal, Canada, where he was involved in research and development activities related to the simulation and analysis of electromagnetic transients. In December 2004, he joined the Faculty of Electrical Engineering, Polytechnique Montréal, where he is currently a Full Professor. Dr. Mahseredjian is a Fellow of the IEEE.